Science Press

ARTICLE

Effect of Hot Working on Microstructures and Mechanical Properties of Gravity-Cast Al-8.3Zn-3.3Cu-2.2Mg High-Strength Aluminum Alloy

Qi Yushi[1],   Jin Yu[1],   Wei Fangming[1],   Du Lanjun[2],   Ren Yan[3],   Liang Xueqian[4],   Chen Gang[1], Du Zhiming[4]

[1] School of Materials Science and Engineering, Harbin Institute of Technology, Weihai, Weihai 264209, China; [2] Beijing Aerospace Propulsion Institute, Beijing 100076, China; [3] Beijing North Vehicle Group Corporation, Beijing 100072, China; [4] School of Materials Science and Engineering, Harbin Institute of Technology, Harbin 150001, China

Abstract: The microstructures and mechanical properties of Al-8.3Zn-3.3Cu-2.2Mg alloys prepared via hot extrusion and liquid forging methods were investigated. Results show that based on DEFORM simulation analysis, the optimal hot extrusion parameters are determined as ingot initial temperature of 380 °C and extrusion speed of 3 mm/s. The hot-extruded aluminum alloy after T6 heat treatment presents superior mechanical properties with yield strength of 519.6 MPa, ultimate tensile strength of 582.1 MPa, and elongation of 11.0%. Compared with the properties of gravity-cast and liquid-forged alloys, the yield strength of hot-extruded alloy increases by 30.8% and 4.9%, and the ultimate tensile strength improves by 43.5% and 10.2%, respectively. The significant improvement in tensile strength of the hot-extruded alloys is attributed to the elimination of casting defects and the refinement of matrix grain and eutectic phases. In addition, the hot-extruded alloy demonstrates superior plasticity compared with the liquid-forged alloy. This is because severe plastic deformation occurs during hot extrusion, which effectively breaks and disperses the eutectic phases, facilitating the dissolution and precipitation of the second phases and inhibiting the microcrack initiation.

Key words: Al-Zn-Cu-Mg alloy; hot extrusion; liquid forging; mechanical properties; microstructure

Al-Zn-Cu-Mg series high-strength aluminum alloys are renowned for their exceptional mechanical properties, including low density, high toughness, and high specific strength, which are extensively used in the aerospace and transportation industries as a promising lightweight material. These alloys are commonly employed in the applications of aircraft fuselage skins, frames, wings, heat exchangers, and automobile engine components[1–3].

The manufacturing process of Al-Zn-Cu-Mg alloys typically includes several steps, such as composition design, casting, homogenization, forming, solution treatment, and aging. The total solute content and the ratios of main alloying elements (Zn, Mg, and Cu) significantly influence the mechanical properties of the Al-Zn-Cu-Mg alloys[4–5]. Increasing the main alloying element content can enhance the solid solution strengthening and precipitation strengthening after heat treatment (HT)[6–8]. Shin et al[9] reported that increasing the fraction of hard phases with high Zn content can improve the hardness and strength of Al-Zn-based alloys. Similarly, Shu et al[10] demonstrated that higher Mg and Cu contents can lead to larger volume fraction of matrix precipitates after aging treatment, resulting in higher strength and hardness. Consequently, adding more main alloying elements through conventional casting methods to prepare ultra-high strength Al-Zn-Cu-Mg alloys becomes the research hotspot[11]. However, increasing the content of alloying elements often results in the formation of coarse eutectic phases in the as-cast alloy[12–13]. These coarse eutectic phases can hardly dissolve into aluminum matrix, which accelerates the initiation and propagation of intergranular crack during deformation[14].

Although conventional casting is effective and can meet the industrial standards, it introduces severe thermal gradients into the ingot, leading to the formation of casting defects, especially hot tears, and cold cracks[15]. As a result, the as-cast Al-Zn-Cu-Mg alloy exhibits undesirable tensile strength and low elongation (EL). Hot working processes, including liquid forging, hot rolling, and hot extrusion, are effective methods for microstructure refinement of as-cast alloys and optimization of mechanical properties. Liquid forging increases the cooling rate of solidification, which enhances the nucleation rate and results in a significant refinement in the grain size of aluminum matrix and the second phases[16–17]. Additionally, plastic deformation through hot working can eliminate casting defects, refine grains and the second phases, and effectively enhances the strength of Al-Zn-Cu-Mg alloys[18].

The hot working processes for aluminum alloys may vary due to their different element composition. In this research, the gravity-cast Al-8.3Zn-3.3Cu-2.2Mg alloy underwent various hot working processes to optimize alloy structures and to enhance mechanical properties. The influence of these hot working methods on the microstructures and mechanical properties of the alloy was investigated.

1 Experiment

The raw material used in this research was the gravity-cast Al-8.3Zn-3.3Cu-2.2Mg alloy. The chemical composition of the gravity-cast alloy was measured by inductively coupled plasma, and the results are presented in Table 1.

The hot extrusion process was simulated using the commercial finite element method (FEM) software DEFORM. Parameters, such as the initial temperature of the casting ingot and extrusion speed, were analyzed and optimized based on the simulation results. The initial temperature parameters for the ingot were set as 360, 370, and 380 °C, and the extrusion speed was set as 1, 3, and 5 mm/s. FEM simulation of the billet and the extrusion dies was conducted using half-symmetry boundary conditions. The extrusion dies consisting of a punch and a container were considered as thermo-rigid state. The minimum mesh element length was 0.98 mm, comprising approximately 35 000 elements in total. The punch travel distance was 68 mm with the step size of 0.33 mm. Heat exchange between workpiece and dies was included in FEM calculations, whereas the heat transfer between the die/extrudate and the surrounding environment was ignored.

A rod-shaped billet with dimension of Φ48 mm×50 mm was cut from the casting ingot for the following hot extrusion treatment. Fig. 1a presents the schematic diagram of hot extrusion die. The extrusion dies were loaded in a servo-hydraulic press and preheated to 380 °C. Colloidal graphite

Table 1 Chemical composition of gravity-cast Al-8.3Zn-3.3Cu-2.2Mg alloy (wt%)

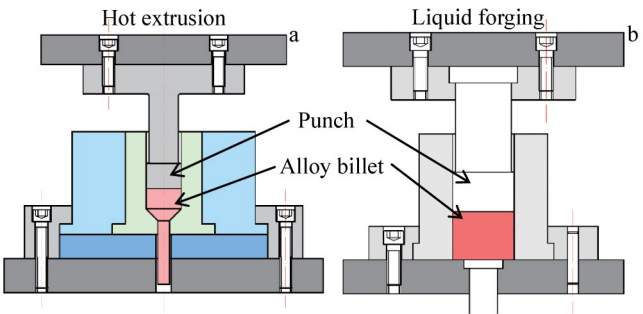| Mg	Zn	Cu	Other	Al
2.22	8.33	3.26	0.96	Bal.

Fig.1 Schematic diagrams illustrating the forming dies of hot extrusion (a) and liquid forging (b)

was applied to the die surface as a lubricant. After homogenization treatment at 465 °C for 24 h, the rod-shaped billet was heated to 380 °C for 6 h and then hot-extruded into a rod (Φ18 mm) with extrusion ratio of 7.1: 1. Subsequently, the hot-extruded rod was water-cooled to room temperature and straightened.

For the liquid forging process, the ingots of 2000 g were melted at 720 °C and isothermally held in a graphite crucible using a resistance furnace. A covering agent was added to the melt surface, and argon gas was continuously introduced into the resistance furnace to prevent oxidization. The C_2Cl_6 powder wrapped with Al foil was added for degassing and refinement. The melt was then poured into the preheated liquid forging dies at 150 °C and then solidified under pressure of 200 MPa for 30 s to ensure the complete solidification. The schematic diagram of the liquid forging die is shown in Fig.1b.

Microstructures were analyzed using optical microscope (OM) and scanning electron microscope (SEM) equipped with energy dispersive spectrometer (EDS). Specimens for SEM analysis were ground and polished. For OM observation, polished specimens were etched by Keller solution (95vol% H_2O, 2.5vol% HNO_3, 1.5vol% HCl, and 1vol% HF). Prior to tensile tests, the specimens underwent T6 HT, which contained solution treatment and artificial aging treatment. Initially, the specimen was held at 465 °C for 2 h for the solution treatment and then underwent immediate water quenching. Subsequently, the specimen was subjected to artificial aging by heating at 120 °C for 24 h and then air cooling. The tensile specimen was rod-shaped with a gauge diameter of 4 mm and a gauge length of 20 mm. Tensile tests were conducted at room temperature using AG-Xplus mechanical testing machine with constant velocity of 1 mm/min. The average value of more than 3 measurements was recorded under different conditions. The fracture surface of tensile specimens was also examined using SEM.

2 Results and Discussion

2.1 Simulation analysis of hot extrusion process and microstructures of hot-extruded alloy

2.1.1 Simulation analysis of hot extrusion process

The primary aim of the simulation is to assess the

feasibility of hot extrusion by controlling process parameters, especially the initial temperature of ingot and the extrusion speed. During the hot extrusion process, the heating effect resulting from plastic deformation significantly influences the temperature[19]. Simulation results indicate that the ingot reaches higher temperatures during the stable extrusion stage, emphasizing the importance of maintaining the ingot temperature below 500 °C to prevent over-burning phenomenon.

Fig. 2 presents the simulation results of the extrusion temperature fields, extrusion temperature distributions, stress fields, and stress distributions of Al-8.3Zn-3.3Cu-2.2Mg alloy under extrusion speed of 3 mm/s with different initial temperatures of alloy ingots. As shown in Fig. 2a, the contact area of the extruded ingot with the die bearing reaches the high temperature of 485 °C when the initial temperature of alloy ingot is 360 °C. With the increase in initial temperature of ingot to 370 and 380 °C, the corresponding temperatures in this region rise to 491 and 494 °C, respectively (Fig. 2e and 2i). The extrusion temperature distributions reveal a gradual increase in the proportion of the relative high temperature area

above 480 °C of the extruded ingot when the initial temperature of alloy ingot increases from 360 °C to 380 °C.

Simulation results of the stress fields (Fig. 2c–2d, 2g–2h, and 2k–2l) indicate that higher equivalent stress exists in the die bearing region (the red area at the ingot top is related to the shape of extrusion punch and it is ignored in this research). Stress distributions reveal a gradual decrease in the proportion of stress of about 240 MPa in the die bearing area when the initial temperature of ingot increases from 360 °C to 380 °C. Concurrently, the proportion of stress within 275–266 MPa decreases. In conclusion, under the extrusion speed of 3 mm/s, increasing the initial temperature of alloy ingot can appropriately facilitate the extrusion and prevent the alloy over-burning.

Fig. 3 illustrates the simulation results of the extrusion temperature fields, extrusion temperature distributions, stress fields, and stress distributions with initial temperatures of Al-8.3Zn-3.3Cu-2.2Mg alloy ingot of 380 °C under different extrusion speeds. As shown in Fig. 3a–3b, 3e–3f, and 3i–3j, the extrusion speed exerts a significant influence on the
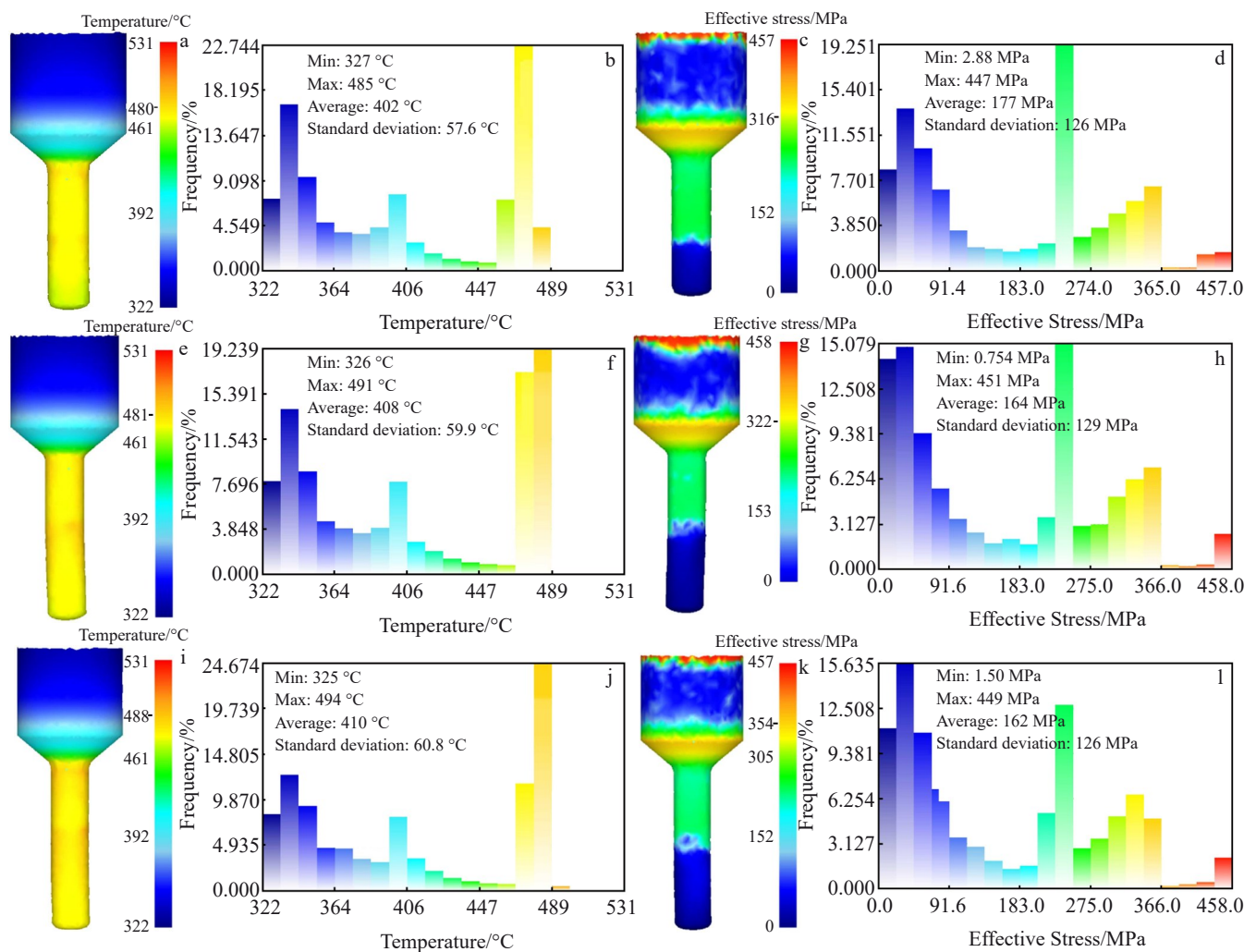

Fig.2 Simulation results of extrusion temperature fields (a, e, i), extrusion temperature distributions (b, f, j), stress fields (c, g, k), and stress distributions (d, h, l) of Al-8.3Zn-3.3Cu-2.2Mg alloy under extrusion speed of 3 mm/s with different initial temperatures of alloy ingot: (a–d) 360 °C; (e–h) 370 °C; (i–l) 380 °C

temperature distribution of extruded alloy. With the increase in extrusion speed from 1 mm/s to 5 mm/s, the maximum temperature on the extruded alloy increases from 419 °C to 519 °C, and the high temperature region is primarily concentrated at the die bearing region. This is because the heat dissipation rate is reduced with the increase in extrusion speed. At the extrusion speed of 5 mm/s, the temperature of localized regions on the extruded alloy exceeds 510 °C, potentially leading to the over-burning during the extrusion process. Therefore, to prevent over-burning, the extrusion speed should be maintained below 5 mm/s when the initial temperature of alloy ingot is 380 °C.

As shown in Fig. 3c – 3d, 3g – 3h, and 3k – 3l, higher equivalent stress (effective stress) also appears in the die bearing region (the red area at the ingot top is related to the shape of extrusion punch and it is ignored in this research). With the increase in extrusion speed from 1 mm/s to 5 mm/s, the maximum equivalent stress on the extruded alloy decreases from 403 MPa to 327 MPa, accompanied by a reduction in the proportion of high stress values. Therefore, appropriately increasing the extrusion speed contributes to the enhancement of extrusion formability.

In conclusion, increasing the initial temperature of alloy ingot and extrusion speed can reduce the equivalent stress during the extrusion process. However, over-high initial temperature and over-fast extrusion speed may lead to over-burning in the localized regions of the extruded alloy. Based on the simulation results, the initial temperature of the ingot is set as 380 °C and the extrusion speed is set as 3 mm/s for the following experiment analysis.

2.1.2　Microstructures of hot-extruded alloy

Fig. 4 presents OM microstructures of the hot-extruded Al-8.3Zn-3.3Cu-2.2Mg alloy along transverse direction (TD) before and after T6 HT. As shown in Fig.4, along TD, the as-extruded alloy is composed of irregular polygonal matrix grains and black second phases. Using image processing software to calculate the average grain size and area fraction of the second phase before and after T6 HT, it is found that the average grain size of the matrix decreases from 47.1 μm to 45.4 μm, whereas the area fraction of the second phase decreases by 49.6%. T6 HT barely influences the shape and size of grains, but significantly affects the quantity and
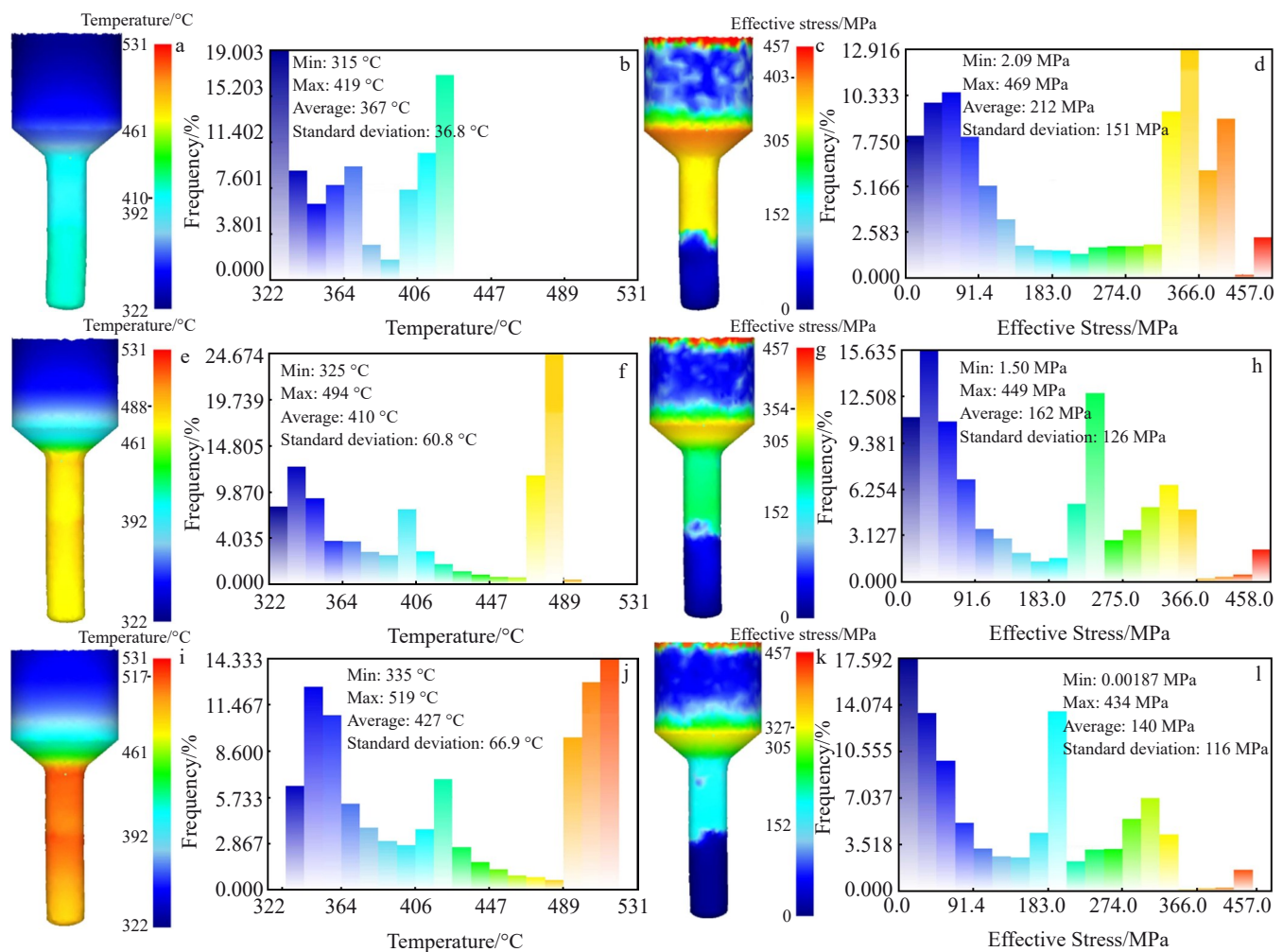

Fig.3　Simulation results of extrusion temperature fields (a, e, i), extrusion temperature distributions (b, f, j), stress fields (c, g, k), and stress distributions (d, h, l) of Al-8.3Zn-3.3Cu-2.2Mg alloy with initial temperatures of alloy ingot of 380 °C under different extrusion speeds: (a–d) 1 mm/s; (e–h) 3 mm/s; (i–l) 5 mm/s
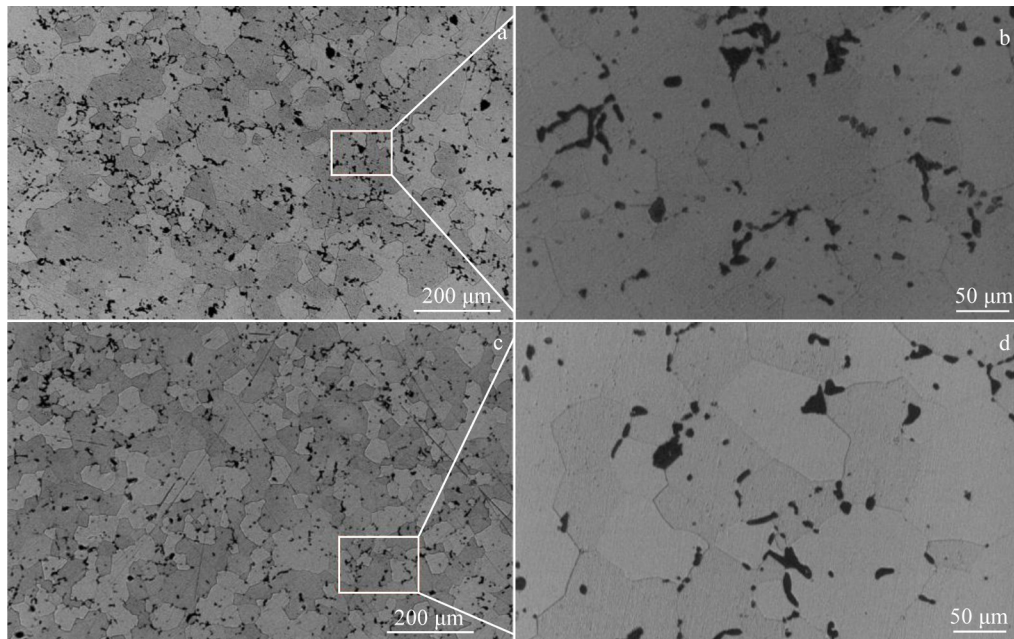
Fig.4 OM microstructures of hot-extruded Al-8.3Zn-3.3Cu-2.2Mg alloy along TD before (a–b) and after (c–d) T6 HT

distribution of the second phases. During the solution treatment process of T6 HT, alloying elements in aluminum alloys gradually dissolve into the alloy matrix, forming a supersaturated solid solution. This phenomenon can be macroscopically observed through the reduction in the second phase content. In the subsequent aging treatment of T6 HT, the alloying elements are precipitated from the supersaturated solid solution to form new strengthening phases. These phases are fine in size and uniformly distributed within the aluminum alloy matrix, significantly enhancing the strength of the aluminum alloy. After T6 HT, the second phases are refined and well dispersed in the aluminum alloy matrix, predominantly distributed at the grain boundaries, and a small number of fine second phase particles are dispersed within the grains.

Fig. 5 shows SEM images and EDS analysis results of the hot-extruded Al-8.3Zn-3.3Cu-2.2Mg alloy before T6 HT along TD and extrusion direction (ED). Homogenization treatment was performed on the Al-Zn-Cu-Mg alloy before hot extrusion to control the element segregation and to eliminate the coarse second phases[20]. However, complete dissolution of intermetallic phases forming during solidification poses challenges[21]. Consequently, the residual second phases are further deformed and broken during hot extrusion. As shown in Fig. 5a, along TD of the extruded rod, the gray second phases with different shapes and sizes are widely distributed in the alloy matrix. As shown in Fig. 5c, the bright second phases are banded along ED, and they are predominantly aggregated along the boundaries of elongated grains. EDS element distributions indicate that these phases

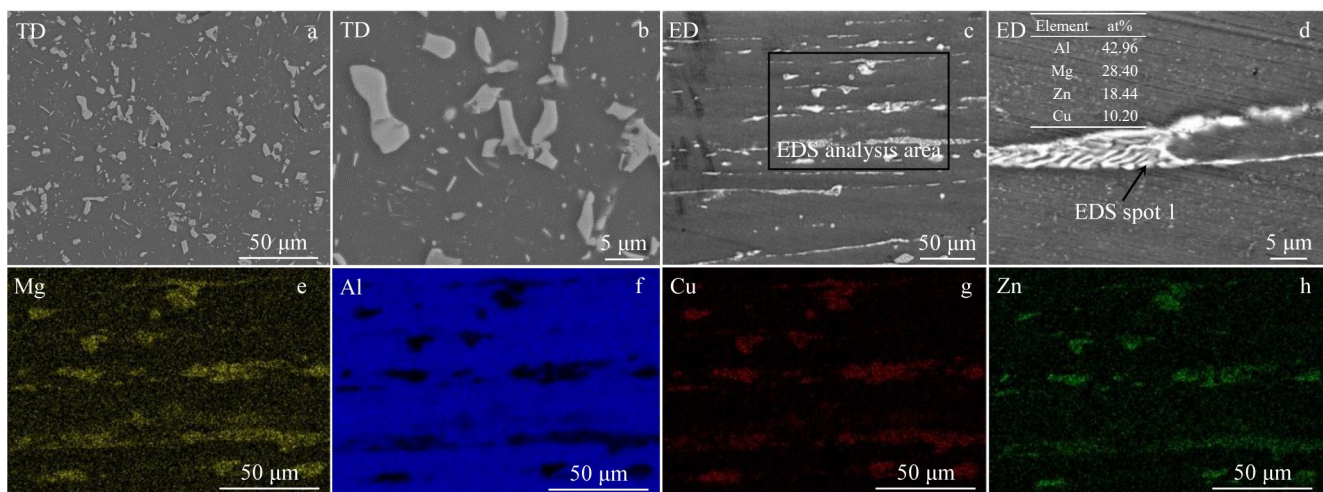| Element	at%
Al	42.96
Mg	28.40
Zn	18.44
Cu	10.20

Fig.5 SEM images with EDS point analysis results (a–d) and EDS element distributions (e–h) of hot-extruded Al-8.3Zn-3.3Cu-2.2Mg alloy before T6 HT along TD (a–b) and along ED (c–d): (e) Mg, (f) Al, (g) Cu, and (h) Zn

mainly consist of Mg, Al, Cu, and Zn elements. As shown in Fig. 5d, some second phases exhibit lamellar structures in the interior area, which is consistent with the results in Ref. [22]. EDS results in Fig. 5d further confirms the presence of Mg(Al, Zn, Cu)$_2$ eutectic.

Fig. 6 shows SEM images of the hot-extruded Al-8.3Zn-3.3Cu-2.2Mg alloy after T6 HT. As shown in Fig. 6, the second phases are significantly refined after T6 HT with the reduction in the number of coarse eutectic phases. However, a small number of the second phases with high melting points remain undissolved, and they are further identified by EDS. The corresponding EDS analysis results are shown in Table 2.

2.2 Microstructures of liquid-forged alloy

SEM images and EDS line scanning analysis results of the liquid-forged Al-8.3Zn-3.3Cu-2.2Mg alloy billet before T6 HT are presented in Fig. 7. As shown in Fig. 7a, the microstructure of liquid-forged Al-8.3Zn-3.3Cu-2.2Mg alloy has non-dendritic grain structures, primarily consisting of polygonal grains and short columnar grains. According to Fig. 7c−7d, the line scanning analysis results across the grain boundary indicate the homogeneous distribution of alloying elements inside the grain with high concentrations of Mg, Cu, and Zn at the grain boundary. Additionally, some lamellar eutectic phases are distributed at the grain boundaries, indicating the formation of Mg(Al, Zn, Cu)$_2$ eutectic. Compared with Zn element, Cu and Mg have lower solubility in the aluminum alloy. During the solidification process of

liquid forging, Cu and Mg are more prone to precipitation at grain boundaries, eventually forming a network of eutectic phases after solidification. If the eutectic phases are not sufficiently dissolved into the aluminum matrix during the subsequent solution treatment, the contents of alloying elements in the matrix would be reduced, further leading to the reduction in strengthening precipitates during aging treatment and thereby impeding the enhancement effect of HT on the alloy strength. The GPII zone and η' phase ($Mg_xZn_yAl_z$) are the main strengthening precipitates of Al-Zn-Cu-Mg alloys. The precipitation sequences in Al-Zn-Cu-Mg alloys are as follows: supersaturated solid solution→GP zones→η'→η (MgZn$_2$).

Fig. 8 shows OM microstructures of Al-8.3Zn-3.3Cu-2.2Mg alloys prepared by gravity casting and liquid forging after T6 HT. As shown in Fig. 8b, the black shrinkage cavity defects (indicated by white arrows) can be detected in the gravity-cast microstructure. During the final stage of solidification, dendrites interconnect, improving the mechanical strength to a certain extent, but the melt is still insufficient to fill the interspace between dendrites. Moreover, thermal stresses within the ingot may initiate microcracks[15]. The sizes of matrix grain and the second phases vary greatly with the second phases mainly distributed along the grain boundaries and less precipitated inside the grains. Fig. 8c–8d illustrate that the liquid-forged microstructure primarily consists of rosette and polygonal grains with uniform distribution and signifi-
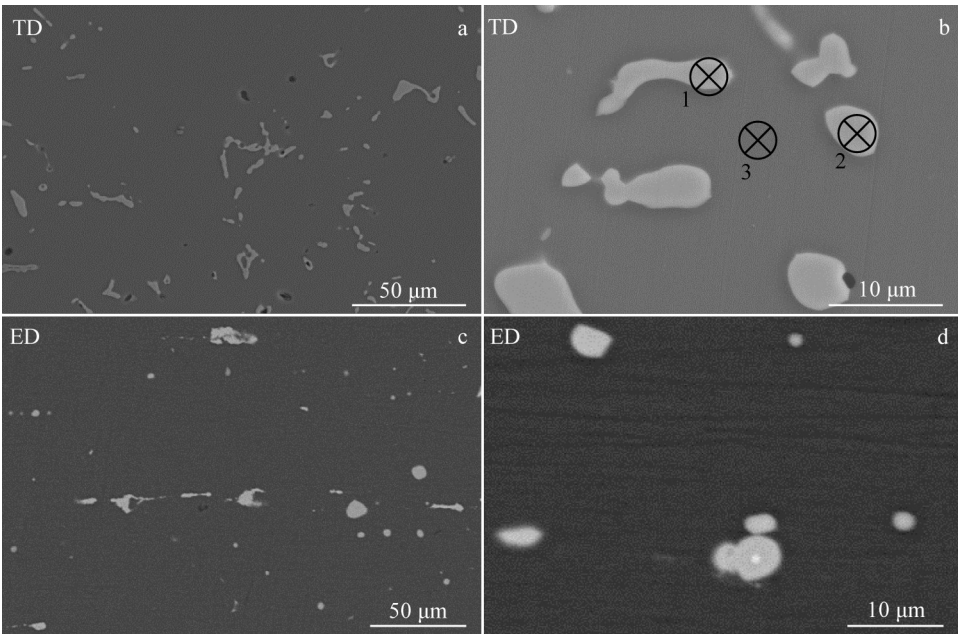

Fig.6   SEM images of hot-extruded Al-8.3Zn-3.3Cu-2.2Mg alloy after T6 HT along TD (a–b) and ED (c–d)

Table 2   EDS analysis results of points marked in Fig.6b (at%)

Point	Mg	Al	Si	Cu	Zn
1	24.33	35.10	0.34	15.94	24.29
2	27.74	28.65	0.38	15.66	27.57
3	2.29	91.53	0.00	0.93	5.25

cantly reduced sizes, compared with that of the gravity-cast microstructure. During liquid forging process, specific pressure facilitates the global liquid feeding and plastic deformation, promoting the elimination of most shrinkage cavities and microcracks. The average grain size of the aluminum alloy decreases from 74.7 μm (gravity casting) to
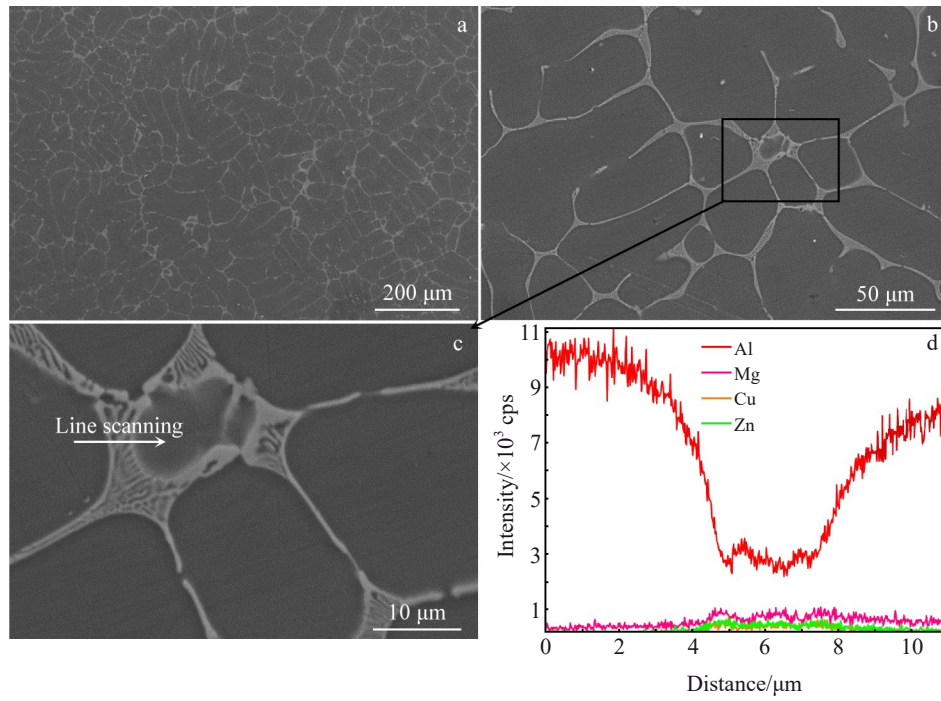
Fig.7 SEM images (a–c) and EDS line scanning results (d) of liquid-forged Al-8.3Zn-3.3Cu-2.2Mg alloy billet before T6 HT
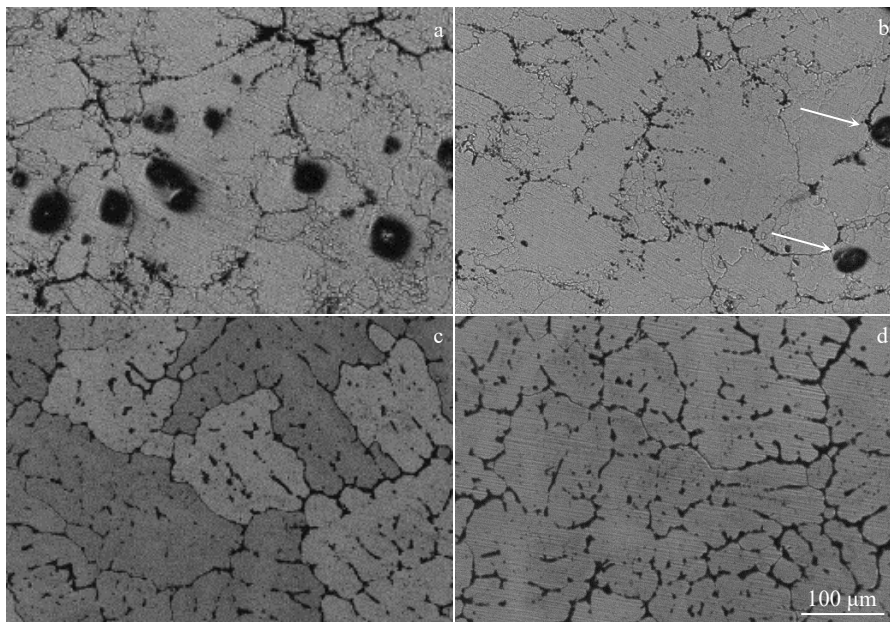

Fig.8 OM microstructures of gravity-cast (a–b) and liquid-forged (c–d) Al-8.3Zn-3.3Cu-2.2Mg alloys after T6 HT

43.9 μm (liquid forging). Due to the refinement of grains in Al-8.3Zn-3.3Cu-2.2Mg alloy matrix after liquid forging, the specific surface area of the grain boundaries increases. Consequently, the average thickness of the eutectic network decreases, which increases the diffusion rate of alloying elements from the eutectic structure into the matrix. During the solution treatment, more alloying elements dissolve into the matrix, forming a greater number of supersaturated solid solutions. This phenomenon promotes an increase in the number of precipitates after aging treatment, thereby

enhancing the strength of aluminum alloy after T6 HT.

2.3 Mechanical properties

Fig. 9 shows the mechanical properties of gravity-cast, hot-extruded, and liquid-forged Al-8.3Zn-3.3Cu-2.2Mg alloys after T6 HT. After T6 HT, the yield strength (YS), ultimate tensile strength (UTS), and EL of the gravity-cast alloy are 397.1 MPa, 405.6 MPa, and 0.5%, respectively. YS and UTS of the hot-extruded alloy are 519.6 and 582.1 MPa, which increase by 30.8% and 43.5%, respectively, compared with those of the gravity-cast alloy. YS and UTS of the liquid-
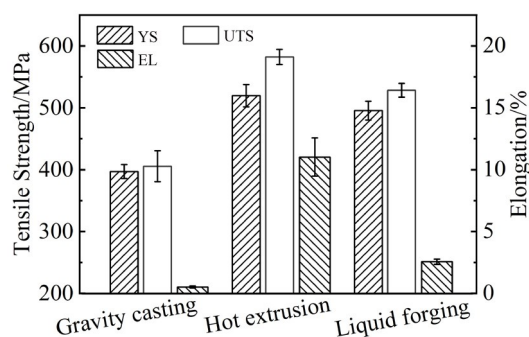
Fig.9 Mechanical properties of gravity-cast, hot-extruded, and liquid-
        forged Al-8.3Zn-3.3Cu-2.2Mg alloys after T6 HT

forged alloy are 495.3 and 528.2 MPa, which increase by 24.7% and 30.2%, respectively, compared with those of the gravity-cast alloy. Both hot-extruded and liquid-forged alloys exhibit significantly improved EL and tensile strength, compared with the gravity-cast alloy. Results reveal that the hot-extruded alloy with higher EL and tensile strength are suitable for the industrial applications due to their better comprehensive properties. Briefly, compared with the properties of gravity-cast and liquid-forged alloys, YS of hot-extruded alloy increases by 30.8% and 4.9%, and UTS improves by 43.5% and 10.2%, respectively.

Fig. 10 shows SEM fracture morphologies of the gravity-cast, hot-extruded, and liquid-forged Al-8.3Zn-3.3Cu-2.2Mg alloys after T6 HT. As shown in Fig. $10a_1 - 10a_2$, the fracture morphologies of the gravity-cast alloy primarily consist of irregular fracture platforms, exhibiting brittle fracture characteristic, which mainly results from the fracture of dendritic arms. The fracture surface exhibits unevenly distributed particles and large clusters of the second phases. Some eutectic precipitates with lower melting points (Al_2Cu

and $MgZn_2$) solidify in the final stage. These eutectic phases are inhibited by grain growth and segregated at grain boundaries, forming a brittle eutectic network after solidification[23]. Eliminating such a eutectic network completely through HT is a great challenge.

As shown in Fig. $10b_1 - 10b_2$, the fracture morphologies of the hot-extruded alloy primarily consist of steps, small dimples, and tearing ridges, indicating a mixed quasi-cleavage and dimple morphology. Dimples originate from the pullout of banded grains with small dispersive particles detected in dimple-near regions. More dimples existing in the fracture morphology suggest higher plasticity. As shown in Fig. $10c_1 - 10c_2$, the fracture morphologies of the liquid-forged alloy mainly consist of lamellar tearing fractures and a few intergranular fractures, exhibiting quasi-cleavage and brittle fracture characteristics.

As shown in Fig.11, the gravity-cast Al-8.3Zn-3.3Cu-2.2Mg alloy exhibits dendritic microstructure with a few casting shrinkage cavities defects. The relatively wide eutectic phases have a continuous distribution between the dendrites. After T6 HT, the eutectic phases are difficult to completely dissolve, and some portions remain at the grain boundaries. During tensile testing, casting defects easily serve as sources for initial microcracks. Under external stress, the coarse undissolved eutectic phases are resistant to plastic deformation and tend to fracture or separate from the aluminum matrix, initiating and propagating cracks along grain boundaries until alloy fracture occurs, which results in significant deterioration of the comprehensive mechanical properties[24].

During hot extrusion, most casting defects, such as microcracks and shrinkage cavities, are ameliorated under heat effect and compressive stress. Gravity-cast dendritic grains undergo fracture and deformation, significantly
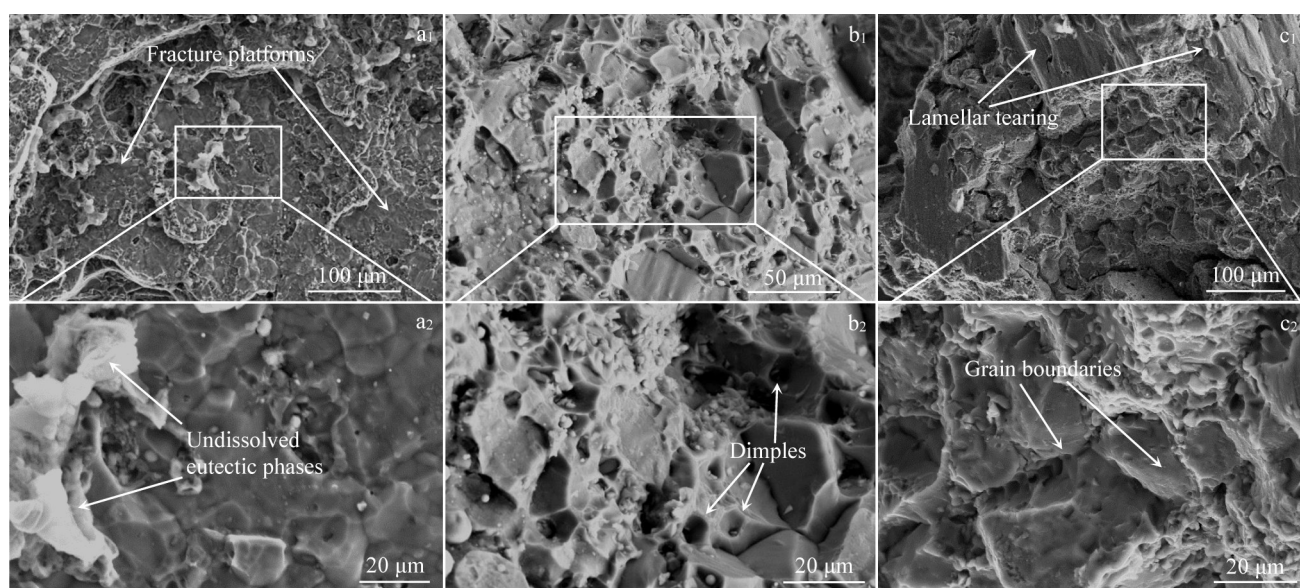

Fig.10 SEM fracture morphologies of gravity-cast (a_1-a_2), hot-extruded (b_1-b_2), and liquid-forged (c_1-c_2) Al-8.3Zn-3.3Cu-2.2Mg alloys after T6
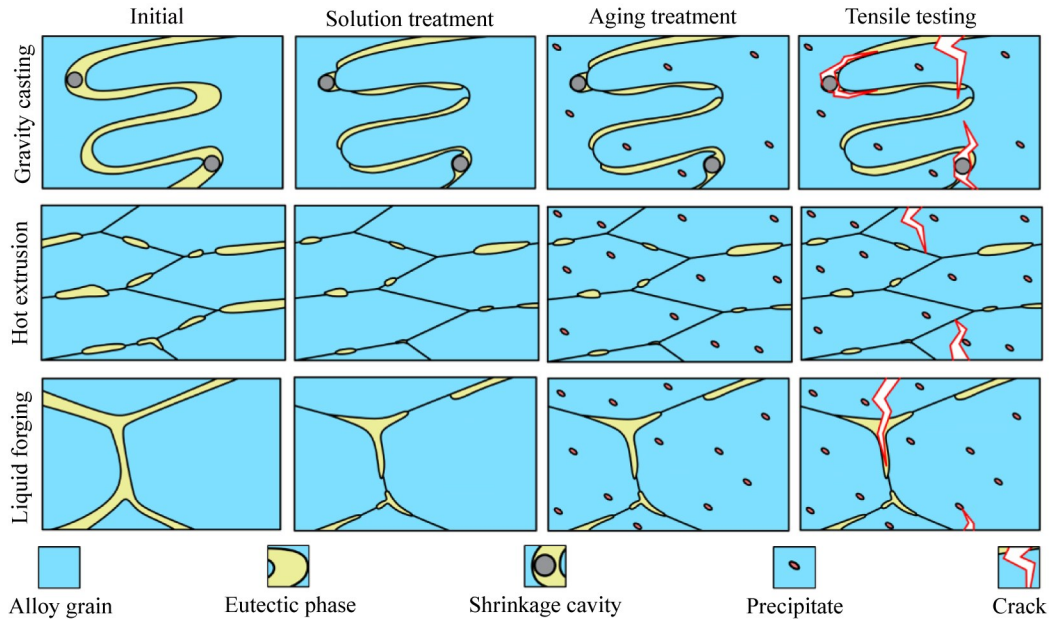   HT

Fig.11 Schematic diagrams of microstructure evolution of Al-8.3Zn-3.3Cu-2.2Mg alloys prepared by different methods during T6 HT and room temperature tensile processes

increasing the grain density. The coarse eutectic phases are fully broken and dispersed along the extrusion direction, and most eutectic phases dissolve into the aluminum matrix after T6 HT. During tensile testing, uniform deformation leads to the same deformation variable exerted on more grains, reducing excessive local stress concentration and inhibiting premature crack generation and development. Multiplication and entanglement of dislocations at grain boundaries during hot extrusion hinder the dislocation migration and microcrack propagation. Fine eutectic phases diminish the crack initiation probability. Sufficient dissolution of eutectic phases during the solution treatment results in the generation of fine and uniformly distributed precipitates during aging treatment. Dislocations are stacked around the dispersed precipitates, impeding further dislocation movement and crack propagation via different mechanisms, such as dislocation shearing of precipitates and Orowan dislocation bypassing[25]. In conclusion, compared with those of the gravity-cast alloy, the strength and plasticity of the hot-extruded alloy are significantly improved.

During liquid forging, specific pressure is applied to the solidified aluminum melt, effectively eliminating the shrinkage cavities and other casting defects, and thereby enhancing the comprehensive mechanical properties. Additionally, this specific pressure positively influences the elevation of liquidus temperature of the melt. The degree of undercooling is promoted during solidification, thereby enhancing the driving force of crystallization[26]. Consequently, liquid forging plays a crucial role in the acceleration of nucleation rate and further refinement of the solidification structures. The grain structure of the Al-8.3Zn-3.3Cu-2.2Mg alloy undergoes a transition from dendritic grain to mixed structure of rosette and polygonal grain. The grain

refinement induced by liquid forging not only enhances the strength of the alloy but also improves its plasticity. The remaining brittle eutectic phases at grain boundaries after T6 HT serve as the fracture origin in tensile testing, resulting in low plasticity of the liquid-forged alloy. Another contribution factor to the low plasticity is the work hardening effect induced by solid feeding. Alloys require more liquid and solid feeding to accommodate the significant shrinkage in the mushy zone during liquid forging.

3 Conclusions

1) For the gravity-cast Al-8.3Zn-3.3Cu-2.2Mg alloy, the optimal HT parameters are initial temperature of ingot as 380 °C and extrusion speed of 3 mm/s.

2) Both hot-extruded and liquid-forged Al-8.3Zn-3.3Cu-2.2Mg alloys demonstrate excellent tensile strength. Particularly, the hot-extruded alloy exhibits higher tensile strength and plasticity: YS, UTS, and EL are 519.6 MPa, 582.1 MPa, and 11.0%, respectively. Compared with those of the gravity-cast alloy, YS and UTS of the hot-extruded alloy increase by 30.8% and 43.5%, respectively.

3) The hot extrusion and liquid forging processes effectively eliminate most casting defects and refine the grains and coarse eutectic phases. This refinement significantly improves the mechanical properties of HTed alloy. However, during liquid forging, the generation of eutectic phase network poses challenges of their complete dissolution into the alloy, thus reducing plasticity. In contrast, the eutectic phases in the hot-extruded alloy suffer sufficient breakage and dispersion under severe plastic deformation, which contributes to the reduction of microcrack initiation and the dissolution and precipitation of the second phases during HT, ultimately enhancing the comprehensive properties of the hot-extruded alloy.

References

1 Williams J C, Starke E A. *Acta Materialia*[J], 2003, 51(19): 5775

2 Nie X J, Chen Z, Qi Y *et al. Acta Metallurgica Sinica (English Letters)*[J], 2023, 36: 1454

3 Wang C C, Guo M X, Yu K C *et al. Materials Characterization*[J], 2022, 193: 112295

4 Zhang Z R, Li Y, Liu Y H *et al. Materials Letters*[J], 2023, 347: 134640

5 Chen Z Y, Mo Y K, Nie Z R. *Metallurgical and Materials Transactions A*[J], 2013, 44: 3910

6 Zou X L, Yan H, Chen X H. *Transactions of Nonferrous Metals Society of China*[J], 2017, 27(10): 2146

7 Zou Y, Wu X D, Tang S B *et al. Transactions of Nonferrous Metals Society of China*[J], 2022, 32(10): 3182

8 Yuan D L, Chen S Y, Chen K H *et al. Transactions of Nonferrous Metals Society of China*[J], 2021, 31(8): 2220

9 Shin S S, Lim K M, Park I M. *Journal of Alloys and Compounds*[J], 2016, 671: 517

10 Shu W X, Hou L G, Zhang C *et al. Materials Science and Engineering A*[J], 2016, 657: 269

11 Jiang H T, Xing H, Xu Z H *et al. Journal of Alloys and Compounds*[J], 2023, 947: 169246

12 Yin H, Wen K, Li Z H *et al. Journal of Materials Research and Technology*[J], 2023, 26: 3646

13 Kang K J, Jiang S D, Li D Y *et al. Materials Characterization*[J], 2023, 200: 112906

14 Ghiaasiaan R, Zeng X C, Shankar S. *Materials Science and Engineering A*[J], 2014, 594: 260

15 Subroto T, Eskin D G, Miroux A *et al. Metallurgical and Materials Transactions A*[J], 2021, 52: 871

16 Wang F F, Meng W, Zhang H W *et al. Transactions of Nonferrous Metals Society of China*[J], 2018, 28(10): 1920

17 Shin S S, Lee J C, Park I M. *Materials Science and Engineering A*[J], 2017, 690: 177

18 Meng X N, Zhang D T, Zhang W W *et al. Journal of Alloys and Compounds*[J], 2020, 819: 152990

19 Kingstedt O T, Lloyd J T. *Mechanics of Materials*[J], 2019, 134: 176

20 Wang Z P, Geng J W, Xia P K *et al. Materials Characterization*[J], 2023, 195: 112531

21 Huang R S, Yang H F, Sun P *et al. Corrosion Science*[J], 2023, 223: 111461

22 Chang X S, Chen G, Sun W *et al. Journal of Alloys and Compounds*[J], 2021, 886: 161254

23 Tang J W, Wang Y R, Jiang Y *et al. Acta Metallurgica Sinica (English Letters)*[J], 2022, 35: 1572

24 Liu G, Sun J, Nan C W *et al. Acta Materialia*[J], 2005, 53(12): 3459

25 Khan M A, Xu C H, Hamza M *et al. Journal of Materials Research and Technology*[J], 2023, 22: 696

26 Liu T, Wang Q D, Sui Y D *et al. Journal of Materials Science Technology*[J], 2016, 32(4): 298

热加工对铸态Al-8.3Zn-3.3Cu-2.2Mg高强铝合金显微组织和力学性能的影响

綦育仕[1]，靳　钰[1]，魏方鸣[1]，杜兰君[2]，任　雁[3]，梁学谦[4]，陈　刚[1]，杜之明[4]

(1. 哈尔滨工业大学（威海）材料科学与工程学院，山东 威海 264209)

(2. 北京航天动力研究所，北京 100076)

(3. 北京北方车辆集团有限公司，北京 100072)

(4. 哈尔滨工业大学 材料科学与工程学院，黑龙江 哈尔滨 150001)

摘　要： 研究了采用热挤压和液态模锻法制备的Al-8.3Zn-3.3Cu-2.2Mg合金的显微组织和力学性能。结果表明：基于DEFORM模拟分析结果，最佳的热挤压工艺参数为铸锭初始温度380 ℃和挤压速度3 mm/s。T6热处理后的热挤压铝合金表现出优异的力学性能，其屈服强度、抗拉伸强度和延伸率分别为519.6 MPa、582.1 MPa和11.0%。与铸态和液态模锻合金相比，热挤压合金的屈服强度分别提高了30.8%和4.9%，抗拉伸强度分别提高了43.5%和10.2%。热加工合金抗拉伸强度显著提升的原因在于热加工过程消除了组织中的铸造缺陷，细化了基体晶粒组织和共晶组织。此外，热挤压合金相比液态模锻合金表现出更加优异的塑性，这是由于热挤压过程中发生剧烈塑性变形，有效破碎并分散了共晶组织，促进第二相的溶解和沉淀析出，并抑制了微裂纹的萌生。

关键词： Al-Zn-Cu-Mg合金；热挤压；液态模锻；力学性能；微观组织

作者简介：綦育仕，男，1991年生，博士，副教授，哈尔滨工业大学（威海）材料科学与工程学院，山东 威海 264209，E-mail：qys_gd@sina.cn